Tetrameric Assembly of CHIP28 Water Channels in Liposomes and Cell Membranes: A Freeze–Fracture Study

Jean-Marc Verbavatz, Dennis Brown, Ivan Sabolić, Giovanna Valenti, D. A. Ausiello, Alfred N. Van Hoek,* Tonghui Ma,* and A. S. Verkman*

Renal Unit, Massachusetts General Hospital and Departments of Medicine and Pathology, Harvard Medical School, Boston, Massachusetts 02114; and *Departments of Medicine and Physiology, Cardiovascular Research Institute, University of California, San Francisco, California 94143-0532

Abstract. Channel forming integral protein of 28 kD (CHIP28) functions as a water channel in erythrocytes, kidney proximal tubule and thin descending limb of Henle. CHIP28 morphology was examined by freeze–fracture EM in proteoliposomes reconstituted with purified CHIP28, CHO cells stably transfected with CHIP28k cDNA, and rat kidney tubules. Liposomes reconstituted with HPLC-purified CHIP28 from human erythrocytes had a high osmotic water permeability (P_f 0.04 cm/s) that was inhibited by $HgCl_2$. Freeze–fracture replicas showed a fairly uniform set of intramembrane particles (IMPs); no IMPs were observed in liposomes without incorporated protein. By rotary shadowing, the IMPs had a diameter of 8.5 ± 1.3 nm (mean ± SD); many IMPs consisted of a distinct arrangement of four smaller subunits surrounding a central depression. IMPs of similar size and appearance were seen on the P-face of plasma membranes from CHIP28k-transfected (but not mock-transfected) CHO cells, rat thin descending limb (TDL) of Henle, and S3 segment of proximal straight tubules. A distinctive network of complementary IMP imprints was observed on the E-face of CHIP28-containing plasma membranes. The densities of IMPs in the size range of CHIP28 IMPs, determined by nonlinear regression, were (in IMPs/μm^2): 2,494 in CHO cells, 5,785 in TDL, and 1,928 in proximal straight tubules; predicted P_f, based on the CHIP28 single channel water permeability of 3.6×10^{-14} cm^3/s (10°C), was in good agreement with measured P_f of 0.027 cm/s, 0.075 cm/s, and 0.031 cm/s, respectively, in these cell types. Assuming that each CHIP28 monomer is a right cylindrical pore of length 5 nm and density 1.3 g/cm^3, the monomer diameter would be 3.2 nm; a symmetrical arrangement of four cylinders would have a greatest diameter of 7.2 nm, which after correction for the thickness of platinum deposit, is similar to the measured IMP diameter of ~8.5 nm. These results provide a morphological signature for CHIP28 water channels and evidence for a tetrameric assembly of CHIP28 monomers in reconstituted proteoliposomes and cell membranes.

CHANNEL forming integral protein of 28 kD (CHIP28)[1] is an abundant integral membrane glycoprotein that was isolated from human erythrocytes (Denker et al., 1988; Smith and Agre, 1991) and recently cloned from human fetal liver (Preston and Agre, 1991) and rat kidney (Deen et al., 1992; Zhang et al., 1993*a*). There is strong evidence that CHIP28 is an important transmembrane water transporting protein in epithelial cells of some segments of the mammalian nephron, as well as in other tissues. Oocytes expressing CHIP28 and liposomes reconstituted with purified CHIP28 protein have a high water permeability that is inhibited by $HgCl_2$ (Preston et al., 1992; Van Hoek and Verkman, 1992; Zeidel et al., 1992). The CHIP28 channel is selective for the passage of water; the transport of urea, monovalent ions, and protons is not increased by expression or reconstitution of CHIP28. In situ hybridization studies indicate that mRNA encoding CHIP28 (or closely homologous proteins) is present in kidney proximal tubule, thin limb of Henle, lung alveolus, intestinal crypt, corneal endothelium, and other tissues (Hasegawa et al., 1993); antibody staining in kidney sections shows that the CHIP28 protein is concentrated in plasma membranes in proximal tubules and thin descending limbs of Henle, both of which have a high constitutive permeability to water (Nielsen et al., 1993; Sabolic et al., 1992).

The structure of CHIP28 in membranes has not been established. Hydropathy analysis suggests multiple hydrophobic membrane-spanning domains: the presence of multiple α-helical domains is supported by spectroscopic analysis of secondary structure by circular dichroism and Fourier transform infrared spectroscopy (Van Hoek et al., 1993). Several

1. *Abbreviations used in this paper*: CHIP28, channel forming integral protein of 28 kD; E, exoplasmic; HPLC, high performance liquid chromatography; IMP, intramembrane particles; MIP, major intrinsic protein; P, protoplasmic; TDL, thin descending limbs.

lines of evidence suggest that CHIP28 monomers are tightly associated as oligomers, including SDS-PAGE analysis of glutaraldehyde cross-linked CHIP28 and sedimentation analysis of detergent-solubilized CHIP28 (Smith and Agre, 1991). In addition, the elution profile for detergent-solubilized CHIP28 by size exclusion HPLC indicated mostly dimers (Van Hoek et al., 1993). However, the target size of ~30 kD determined by radiation inactivation suggests that the functional unit of CHIP28 is the monomer (Van Hoek et al., 1991). Further preliminary evidence for functional CHIP28 monomers comes from coexpression studies of mRNA encoding wild-type and certain mutant CHIP28 proteins in *Xenopus* oocytes (Preston et al., 1993; Zhang et al., 1993*b*); it was found that expression of mutant CHIP28 did not affect the water transporting function of wild-type CHIP28. Therefore, the state of CHIP28 assembly in membranes is not known, nor is it clear whether an oligomeric assembly of CHIP28 is required for water transport function.

It is well established that certain integral membrane proteins are visible as intramembrane particles (IMPs) by freeze–fracture EM. Visualization of IMPs in vasopressin-responsive kidney and amphibian epithelial cells with this technique has provided valuable information about the cell biology of the vasopressin-sensitive water channel (Brown et al., 1983; Chevalier et al., 1974; Harmanci et al., 1978). For some membrane proteins, including the proton ATPase (Humbert et al., 1975; Wade, 1976) and the major intrinsic protein of lens (MIP26) (Dunia et al., 1987; Zampighi et al., 1989), the IMPs display characteristic features and/or regular patterns of organization. The purpose of the present study was to examine the morphology of functional CHIP28 water channels by freeze–fracture EM. The results show that CHIP28 gives rise to IMPs with characteristic morphological features. These IMPs were identified in liposomes reconstituted with purified CHIP28 protein, in CHO cells transfected with CHIP28 cDNA, and in native kidney tubule plasma membranes. The dimensions and shape of the IMPs suggest that CHIP28 forms tetramers in artificial and native membranes.

Materials and Methods

Purification of CHIP28 and Membrane Vesicle Preparation

Human erythrocyte membranes obtained by hypotonic lysis were stripped with KI to remove non-integral proteins and then with 3% *N*-lauroylsarcosine to remove the majority of non-CHIP28 proteins (Van Hoek and Verkman, 1992). The pellet obtained after *N*-lauroylsarcosine stripping was solubilized in 35 mM octylglucoside, and CHIP28 was delipidated and further purified by anion exchange chromatography on a DEAE-sephacel column and by size-exclusion high performance liquid chromatography (HPLC) on a column (G3000SW; TSK America, North Bend, WA) (Van Hoek et al., 1993). CHIP28 was reconstituted into proteoliposomes containing PC, PI, and cholesterol (mole ratio 11:1:11) by detergent dilution to give proteoliposomes with a lipid-to-protein ratio of 4 (wt/wt).

Brush border membrane vesicles were isolated from rat renal cortex by the Mg/aggregation method (Biber et al., 1981).

Transfected CHO Cells

CHO cells were stably transfected with cDNA encoding rat kidney CHIP28k as described previously (Ma et al., 1993). CHO cells were transfected with vector pRc/CMV (Invitrogen, San Diego, CA) alone (mock-transfected cells) or vector containing the coding sequence of CHIP28k. Transfected cells were selected by addition of Geneticin to the medium for 14 d and clonal lines with high CHIP28k expression were identified by immunoblotting. Plasma membrane vesicles from CHO cells were isolated by cell homogenization, followed by differential and sucrose gradient centrifugation (Ma et al., 1993). The plasma membrane marker alkaline phosphodiesterase I was enriched 14-fold compared to the cell homogenate.

SDS-PAGE and Immunoblotting

Membrane proteins from the preparations used for functional and morphological studies were analyzed by SDS-PAGE and Western blot. Vesicles were dissolved in 2% SDS, resolved on 12% SDS-PAGE, and electrotransferred to nitrocellulose for immunoblotting with a rabbit anti-CHIP28 antibody as described previously (Sabolic et al., 1992).

Water Permeability Measurements

Osmotic water permeability in proteoliposomes and plasma membrane vesicles from CHO cells and rat kidney proximal tubule was measured by a stopped-flow light scattering technique (Van Hoek and Verkman, 1992). Vesicles were suspended in 50 mM mannitol, 5 mM Na phosphate, pH 7.4, and subjected to a 50 mM inwardly directed mannitol gradient at 10°C. In some experiments, 0.3 mM $HgCl_2$ was added 5 min before water transport measurements. Water permeability (P_f, cm/s) was calculated from the course of 90° scattered light intensity (520 nm) and vesicle geometry as described previously.

Kidney Tissue Preparation

Rats were anesthetized with Nembutal (0.1 ml of a 50 mg/ml solution per 100 g body weight) and perfused first with HBSS for 2 min and then with a fixative containing 2% glutaraldehyde in PBS for 10 min. Kidneys were isolated, sliced, and kept overnight in fixative at 4°C. Tissue slices were then washed three times in PBS and kept in PBS containing 0.02% NaN_3 at 4°C.

Freeze–fracture Electron Microscopy

Freeze–fracture studies were performed on stripped erythrocyte plasma membrane, proteoliposomes, transfected CHO cells, and rat kidney tissue. Vesicles, cells, or kidney tissue were fixed in 2% glutaraldehyde, washed twice in PBS, and cryoprotected in 30% glycerol in PBS for >1 h. The samples were mounted on 3-mm copper freeze–fracture supports and frozen by immersion in N_2-cooled Freon 22 at −150°C. The specimens were fractured with a knife in a Cressington freeze–fracture apparatus (Cressington Scientific Instruments, Watford, U.K.) at −130°C under a vacuum of 10^{-7} Torr and shadowed with an ~1.5-nm total coat of platinum at 45°, followed by 6 nm of carbon at 90°. The platinum shadowing was performed with or without specimen rotation. The crystal thickness monitor was stationary. The replicas were cleaned in bleach for several hours, followed by chloroform–methanol and water washes. The replicas were collected on formvar-coated copper grids and observed in an electron microscope (CM10; Philips, Mahwah, NJ).

The protoplasmic (P) face IMP and exoplasmic (E) face complementary imprint densities were measured on a plasma membrane surface area >0.02 μm^2 on each micrograph of 6 to 18 different cells. The IMP greatest diameters were measured on micrographs of the replicas printed at a final magnification of 300,000×. IMP size distribution histograms were obtained from 208 to 424 measurements on >15 micrographs in each sample. The IMP density versus size distribution was fitted to unimodal or bimodal Gaussian distributions by non-linear least square regression; fitted parameters are reported in the legend to Fig. 9 and in Table III.

Immunocytochemistry

CHO cells grown on 6-well plates were fixed in 4% paraformaldehyde, 0.1% glutaraldehyde in PBS (PBS pH 7.4) overnight, and stored in PBS containing 0.02% NaN_3.

Immunofluorescence Studies. After rinsing in PBS, cells were permeabilized by addition of 0.1% Triton X-100 (in PBS) for 5 min, washed twice for 5 min in PBS, followed by 5 min in PBS containing 0.2% gelatin. The cells were incubated with anti-CHIP28 rabbit serum (diluted 1:400 in 1% BSA in PBS) for 1 h at room temperature, followed by two 5-min washes in high-salt PBS (containing 2.7% NaCl to decrease nonspecific antibody

binding), and two washes in regular PBS. The samples were incubated for 45 min at room temperature with a fluorescein-conjugated goat anti-rabbit antibody (15 μg/ml in PBS; Calbiochem-Behring Corp., San Diego, CA), washed twice in high-salt PBS, and twice in PBS. Finally, the plastic wells were mounted in 50% glycerol, 0.2% Tris-HCl, pH 8.0, containing 2% *n*-propyl gallate to retard fluorescence quenching. The cells were examined on a confocal microscope (600; Bio-Rad Laboratories, Cambridge, MA), and images were hardcopied on a video printer.

Immunogold Studies. A cell pellet obtained by scraping was infiltrated overnight in 2.3 M sucrose. A drop of pellet was frozen in liquid N_2 and 60 nm ultrathin sections were cut on a Reichert FC4D ultracryomicrotome at −70°C. The sections collected on carbon/Parlodion-coated nickel grids were washed 3 × 5 min in PBS and preincubated 2 × 10 min in 1% BSA in PBS. The grids were then incubated for 90 min in a 1:400 dilution of anti-CHIP28 immune serum in 1% BSA/PBS, washed 2 × 10 min in 1% BSA/PBS, incubated in a 1:50 dilution of 15 nm protein A-gold in 1% BSA/PBS, washed once in 1% BSA/PBS for 10 min and twice in PBS for 5 min. Finally, the sections were fixed in 1% glutaraldehyde in PBS for 20 min, washed twice in water for 5 min, stained, and embedded in 0.2% uranyl acetate, 0.5% methyl cellulose in water for 10 min, and dried. The transfected CHO cell sections were examined and photographed in a Philips CM10 electron microscope.

Results

Biochemical and Functional Characterization of Vesicle Samples

Figs. 1, *a* and *b* show SDS-PAGE and immunoblot of samples used for subsequent morphological studies. The *N*-lauroylsarcosine-stripped erythrocyte membranes (lane *A*) and proteoliposomes reconstituted with CHIP28 (lane *C*) showed the non-glycosylated (at 28 kD) and glycosylated (at 40–70 kD) forms of CHIP28. The plasma membrane fractions isolated from mock-transfected (Fig. 1 *b*, lane *D*) and CHIP28k-transfected (lane *E*) CHO cells showed many proteins on stained gel; however, only the CHIP28-transfected cells showed immunoreactive protein. Similar results were obtained for brush-border membrane vesicles isolated from rat kidney cortex (Fig. 1 *b*, lane *F*), which consist primarily of apical plasma membrane from proximal tubules. The glycosylation pattern of the erythrocyte and kidney forms of CHIP28 were similar.

Fig. 1 *c* shows stopped-flow light scattering analysis of osmotic water permeability (P_f) of the vesicle fractions examined above. The P_f values were used for comparison with measured IMP densities (see below). P_f in *N*-lauroylsarcosine stripped vesicles was high (0.026 cm/s at 10°C) and strongly inhibited by $HgCl_2$. P_f in protein-free liposomes was low (0.006 cm/s) and $HgCl_2$ insensitive, whereas P_f in liposomes reconstituted with purified CHIP28 was high (0.041 cm/s) and $HgCl_2$ sensitive. The single channel water permeability (p_f, in cm^3/s) for CHIP28 monomers, calculated from P_f, and proteoliposome lipid-to-protein ratio and size, was 3.6×10^{-14} cm^3/s at 10°C. In plasma membrane vesicles isolated from CHO cells, P_f was low (0.008 cm/s) and $HgCl_2$ insensitive for mock-transfected cells (not shown), and high (0.027 cm/s) and $HgCl_2$ sensitive in the CHIP28k-transfected cells. In brush-border vesicles from rat proximal tubule, the light scattering data showed a high P_f (0.031 cm/s) that was $HgCl_2$ sensitive.

Characterization of IMPs in Vesicles and Proteoliposomes Containing CHIP28

Freeze–fracture EM of the pellet obtained after KI stripping of erythrocyte membranes showed a heterogeneous population of vesicles (Fig. 2 *a*), ranging from 100 nm to 1 μm in diameter, many of which were multilamellar. These vesicles contained a high density of different sorts of IMPs on both fracture leaflets. The dense packing of the IMPs precluded high-resolution visualization of particle structure.

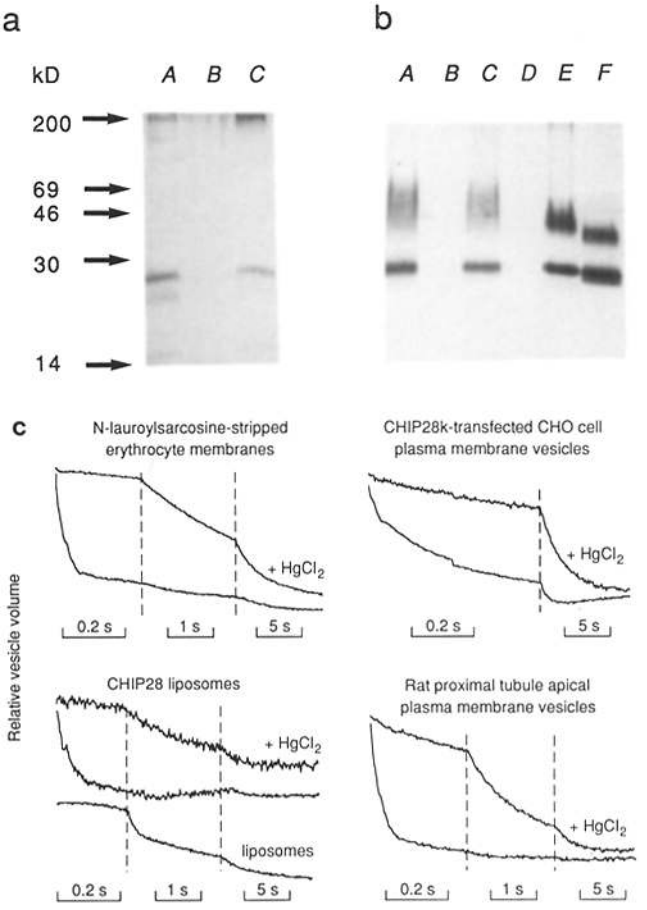

Figure 1. Biochemical and functional analysis of vesicles. (*a*) 12% Laemmli SDS-PAGE with Coomassie blue staining of *N*-lauroylsarcosine– stripped erythrocyte membranes (lane *A*), liposomes (lane *B*), and CHIP28 proteoliposomes (lane *C*). (*b*) Western blot probed with an anti-CHIP28 antibody of *N*-lauroylsarcosine–stripped erythrocyte membranes (lane *A*), liposomes (lane *B*), CHIP28 proteoliposomes (lane *C*), plasma membranes from mock- (lane *D*) and CHIP28k-transfected (lane *E*) CHO cells, and rat kidney apical membrane vesicles (lane *F*), showing non-glycosylated CHIP28 at 28 kD and glycosylated CHIP28 with an apparent molecular size of 40–70 kD. (*c*) Stopped–flow light scattering measurement of osmotic water permeability. Vesicles were mixed with a hyperosmotic solution as described in Materials and Methods and the time course of vesicle shrinkage was measured. Where indicated, 0.3 mM $HgCl_2$ was added at 5 min before the measurement.

After stripping by *N*-lauroylsarcosine, the vesicles had a more homogeneous size (Fig. 2 *b*), with an average diameter of 280 nm, in agreement with the size measured by quasi-elastic light scattering (Van Hoek and Verkman, 1992). As shown in Fig. 1 *a*, CHIP28 was found to comprise >95% of the intramembrane proteins; by freeze–fracture EM, there was a more homogeneous population of IMPs in these vesicles (Fig. 2 *b*). The average diameter of these particles was 8.6 ± 1.7 nm (mean ± SD, 89 IMPs measured). Liposomes

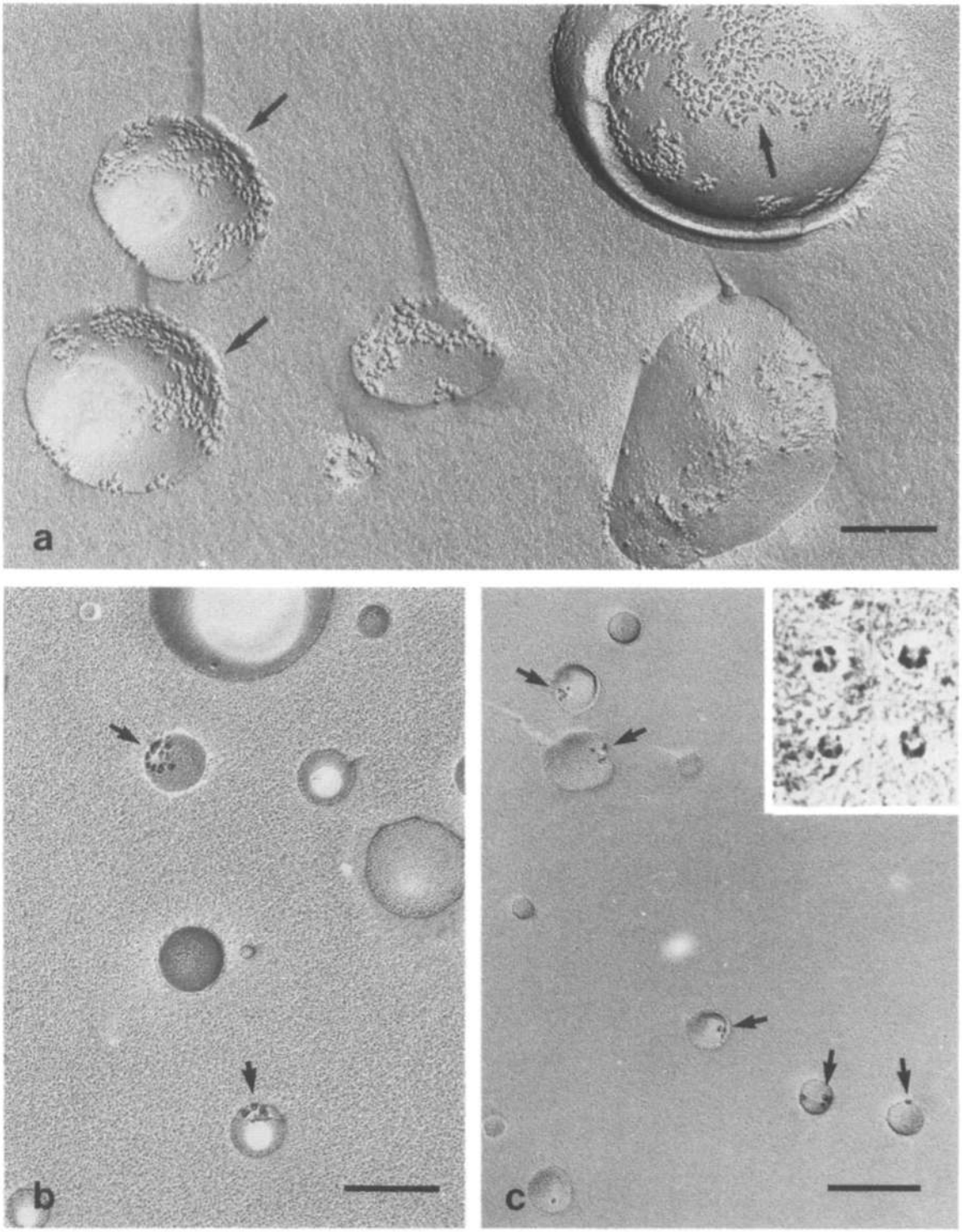

Figure 2. Freeze-fracture of KI-stripped erythrocyte membranes (*a*), *N*-lauroylsarcosine stripped vesicles (*b*), and CHIP28-incorporated proteoliposomes (*c*). Arrows show vesicles containing IMPs. (*Inset*) Gallery of four rotary-shadowed IMPs from CHIP28-incorporated liposomes (×500,000). Note the tetragonal shape of the IMPs. Bars, 150 nm.

reconstituted with purified CHIP28 had an average diameter of 140 nm (Fig. 2 *c*). IMPs observed by freeze-fracture EM were not different in appearance from those observed in the *N*-lauroylsarcosine-stripped vesicles. In rotary shadowed samples and under favorable shadowing and observation conditions, the IMPs of CHIP28 reconstituted proteoliposomes appeared to be square, with a greatest diameter of 8.5 ± 1.3 nm (n = 285). These square IMPs observed on either the external or the internal leaflet of the membrane, often appeared to be tetragonal with an apparent central depression where the platinum shadowing was less dense (Fig. 2 *c*, *inset*). At high magnification, in rotary shadowed samples,

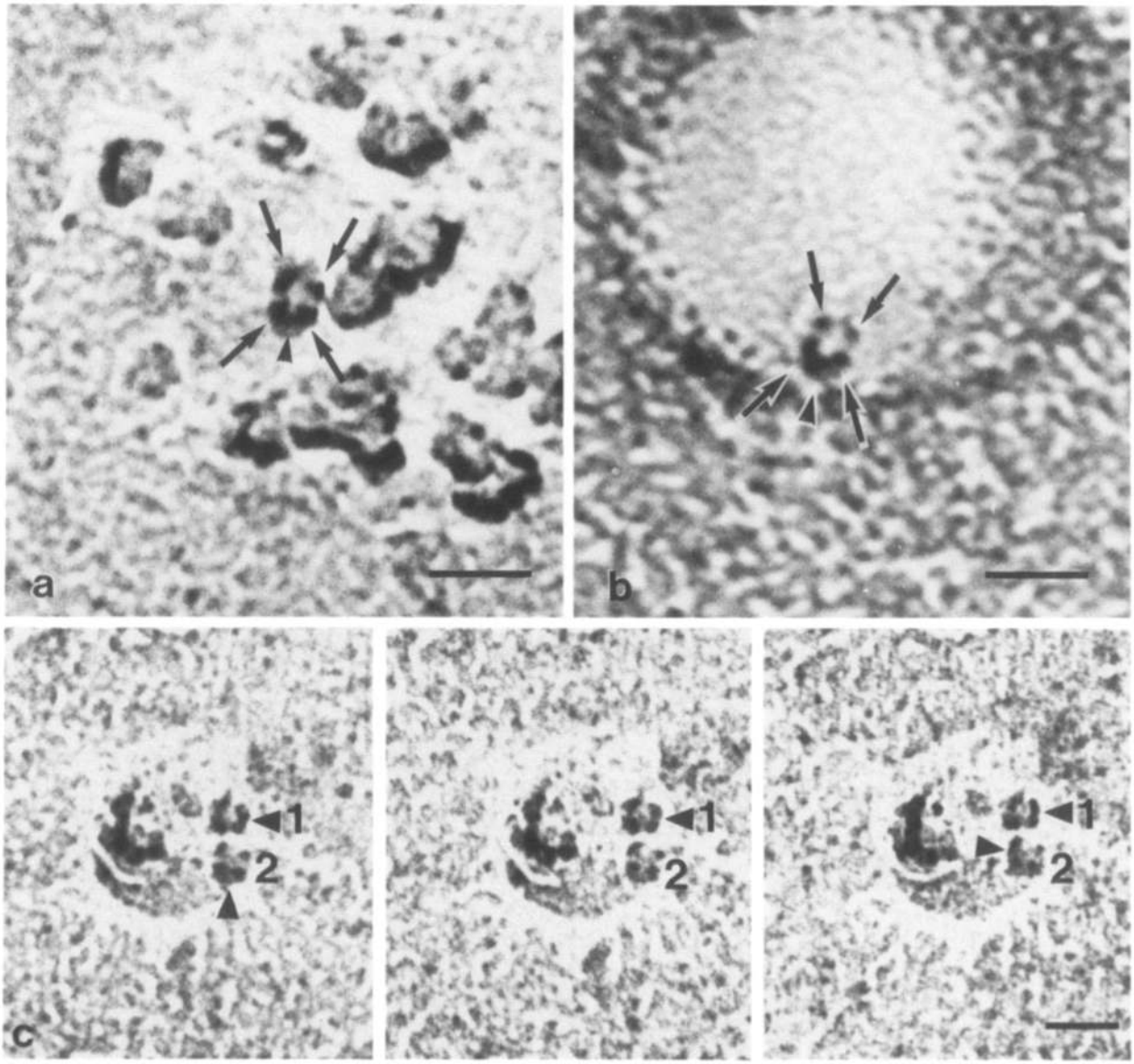

Figure 3. Rotary shadowing freeze–fracture of *N*-lauroylsarcosine stripped vesicles (*a*), CHIP28-incorporated proteoliposome (*b*), and liposome reconstituted with CHIP28 viewed at three different angles of observation, left to right by tilting the specimen on the microscope stage of −5°, 0°, and 10°, respectively (*c*). CHIP28 IMPs are tetramers of ~8.5-nm diam. Arrows show IMP subunits. The subunits are sometimes connected by a dense bridge (*arrowheads*). While the tetrameric structure is visible in IMPs 1 and 2 at all angles of observation, the relationship between subunits appears variable. Bars, 15 nm.

IMPs in *N*-lauroylsarcosine stripped vesicles (Fig. 3 *a*) and proteoliposomes reconstituted with CHIP28 (Fig. 3 *b*) appeared to be composed of four subunits (*arrows*). In many cases, at least two of the subunits appeared to be linked by a bridge of electron-dense material (Fig. 3, *arrowheads*). Fig. 3 *c* shows two IMPs on the membrane of a CHIP28 proteoliposome, photographed at three different angles of observation. A dense bridge is visible on one of the IMPs in each micrograph (Fig. 3 *c*, IMP 1, *arrowheads*), but the appearance of the other IMP (Fig. 3 *c*, IMP 2) is dependent on the angle of observation. Although the four subunits are clearly defined at one angle (Fig. 3 *c*, IMP 2, *center*), two of the subunits are less visible at the two other angles of observation (Fig. 3 *c*, IMP 2, *arrowheads*). The IMP subunit composition was also examined on stereomicrographs obtained by both unidirectional and rotary-shadowing freeze–fracture EM. In some IMPs, subunits and the central depression could be detected without sample rotation on stereomicrographs (Fig. 4 *a*). Fig. 4 *b* demonstrates the increase in resolution obtained with rotary-shadowed samples: the IMP shape appears to be similar, but the IMP details are sharper and the oligomeric assembly is more easily recognized. Due to the curvature of the liposome membrane, particles located on the edge are seen from their side, so that the tetrameric assembly and central depression are not visible. These variations in the appearance of CHIP28 IMPs prevent any conclusion on the origin of the bridge that was often observed between adjacent subunits of CHIP28 tetramers.

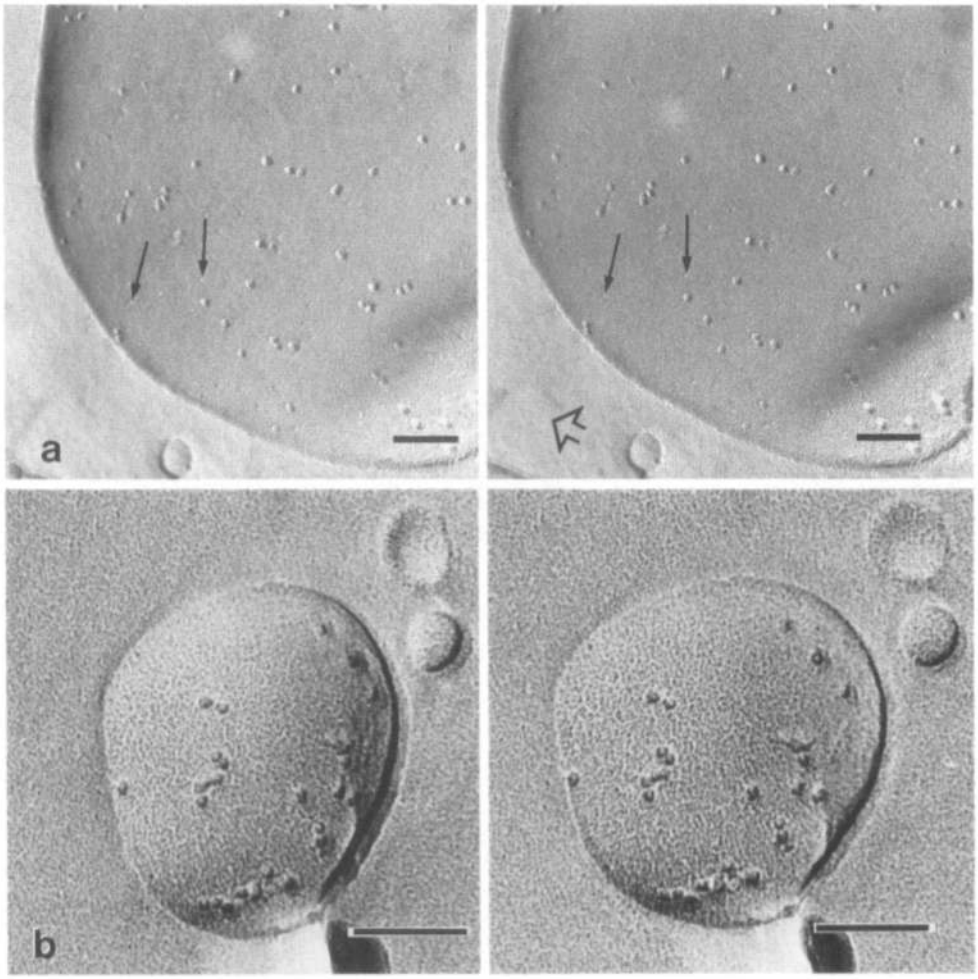

Figure 4. Stereomicrographs of CHIP28-incorporated liposome membranes in freeze-fracture EM by unidirectional shadowing (*a*) and rotary shadowing (*b*). Empty arrow shows direction of platinum shadowing, full arrows show IMP imprints. Visualization of particle structure is enhanced by rotary shadowing, but subunits are only visible on flat membrane areas. Bars, 75 nm.

CHIP28k-transfected Cells

Morphological studies were carried out in CHO cells stably transfected with vector alone (mock transfected) or CHIP28k cDNA (CHIP28k transfected). The presence of the CHIP28k water channel in the plasma membrane of these cells was confirmed by indirect immunofluorescence. Mock and CHIP28k-transfected CHO cells were probed with anti-CHIP28 antibodies raised in rabbit (Sabolic et al., 1992). In CHIP28k-transfected CHO cells, strong antibody staining was observed on the plasma membranes (Fig. 5 *b*), whereas no staining was observed in mock-transfected cells (Fig. 5 *a*). In this clonal population of stably transfected cells, CHIP28k was present on the plasma membranes of every cell, and probably on some intracellular membranes. By immunogold labeling of CHIP28 on ultrathin frozen sections, CHIP28k was localized primarily to plasma membranes in CHIP28k-transfected CHO cells (Fig. 5 *d*), as well as some intracellular membranes, whereas mock-transfected cells were not labeled (Fig. 5 *c*).

By freeze-fracture EM, the size and density of IMPs in the plasma membrane of CHIP28k-transfected (Fig. 6 *b*) and mock-transfected CHO cells (Fig. 6 *c*) differed remarkably. As is often the case, the density of IMPs was higher on the protoplasmic fracture face (P-face). In mock-transfected cells, the IMPs on the plasma membrane P-face were heterogeneous and had an average size of 7.3 $\pm$ 2.0 nm (n = 208). In CHIP28k-transfected cells, the IMPs observed on the P-face of the plasma membranes were larger (8.8 $\pm$ 1.9 nm [n = 247]) and found at higher density than in mock-transfected cells (Table I); they often appeared to form loose clusters. Similar large IMPs were also observed on the P-face of intracellular membranes (Fig. 6 *a*, *arrows*). In rotary shadowed CHIP28k-transfected cells (Fig. 6 *d*), most IMPs on the P-face were similar in appearance to those in proteoliposomes. Under favorable shadowing conditions, a tetrameric structure was observed in many IMPs (Fig. 6 *d*, *arrows*). A quantitative analysis of the IMP size distribution is provided at the end of the results section.

On the exoplasmic fracture face (E-face) of plasma membranes, no difference in IMP distribution was apparent between CHIP28k- and mock-transfected CHO cells. However, a striking modification of the structure of the membrane E-face was observed in CHIP28k-transfected cells. Micrographs of the plasma membrane E-face in CHIP28k-transfected cells showed a distinctive pattern of contrasted imprints of $\sim$2 nm, often found in loose clusters (Fig. 7 *b*, *circle*) that were not seen on the mock-transfected cells (not shown). Probably because of plastic deformation of the membrane E-face and partial filling of the imprints during the fracturing and shadowing process, no substructure was visible in these imprints. These E-face pits usually represent

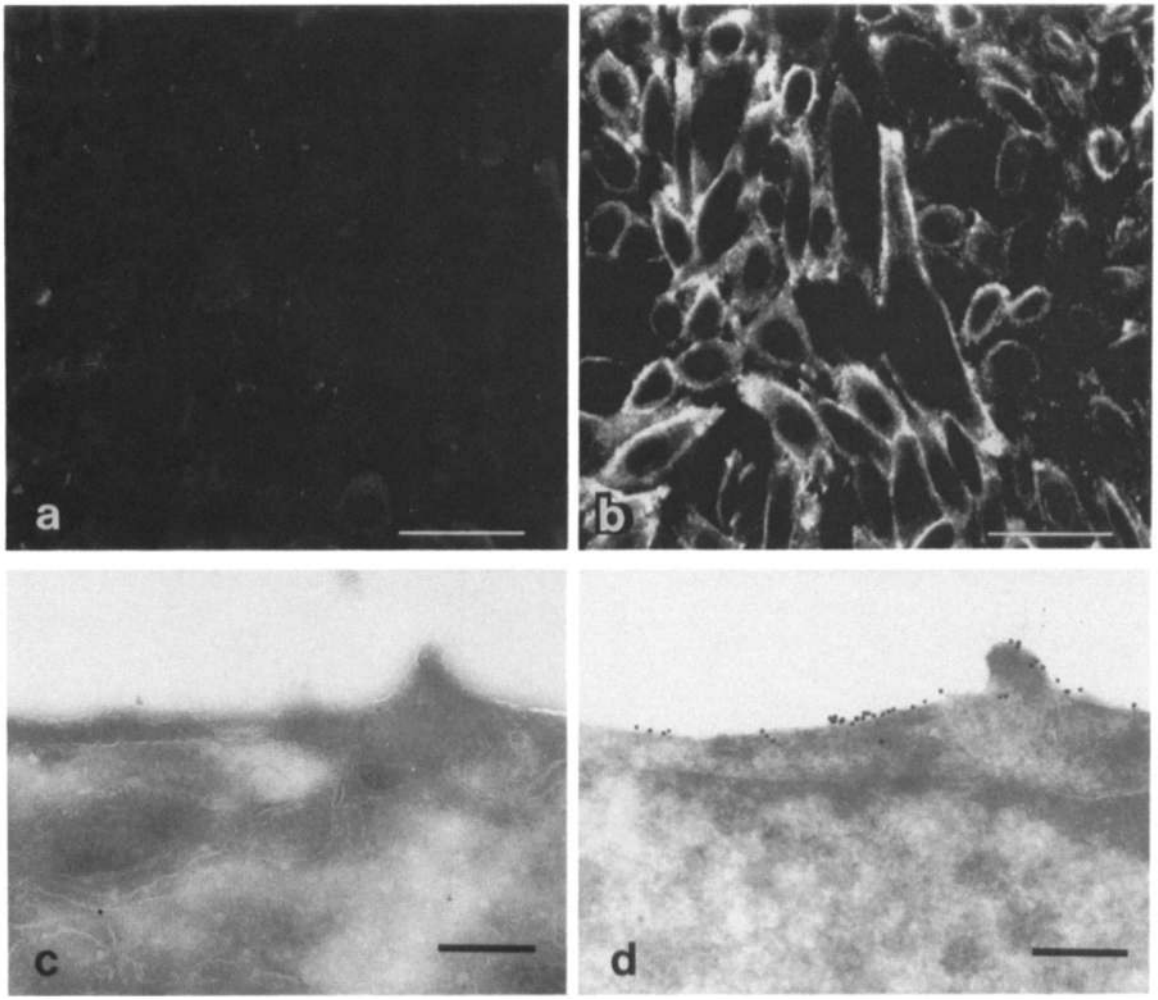

Figure 5. Immunofluorescence anti-CHIP28 staining of mock- (*a*) and CHIP28k-transfected (*b*) CHO cells by confocal microscopy. Immunogold labeling with anti-CHIP28 antibodies on ultrathin frozen sections from mock-transfected CHO cells (*c*) and CHIP28k-transfected cells (*d*). CHIP28k-transfected cell plasma membranes are heavily labeled. Bars: (*a* and *b*) 50 μm; and (*c* and *d*) 0.3 μm.

imprints of complementary IMPs, but not all classes of IMPs leave such an imprint (Verkleij and Ververgaert, 1978). In the CHIP28k-transfected CHO cells, the density of the E-face imprints was similar to the density of P-face IMPs (Table I), supporting the idea that each of the large P-face IMPs representing CHIP28 leaves a single imprint. Accordingly, similar imprints were also observed on the membrane of proteoliposomes reconstituted with CHIP28 (Fig. 4 *a*, *full arrows*).

Water Permeable Kidney Segments

The rat CHIP28k water channel is 94% identical to human erythrocyte CHIP28 (Zhang et al., 1993*a*) and localized primarily to the S2 and S3 segments of the proximal tubule and thin descending limb long loops of Henle (Hasegawa et al., 1993; Nielsen et al., 1993; Sabolic et al., 1992). This localization is in agreement with the high constitutive water permeability of these nephron segments (Chou and Knepper, 1992; Green and Giebisch, 1989; Schafer et al., 1978). By freeze–fracture EM, the apical plasma membrane P-face of the water permeable nephron segments was found to contain a high density of IMPs (Orci et al., 1981). In contrast, the water impermeable ascending limbs and distal tubules contain a markedly lower density of IMPs in their luminal membranes. Based on these observations, it was suggested that there might be a relationship between water permeability and IMP densities in the plasma membrane of these kidney epithelial cells (Orci et al., 1981). We have used rotary-shadowing freeze–fracture EM to compare the IMPs in kidney epithelial cells with those observed in CHIP28-incorporated proteoliposomes and CHIP28k-transfected CHO cells.

Fig. 8 *a* shows a freeze-fracture micrographs of the brush-border membrane of a proximal convoluted tubule. Although some tetrameric IMPs were observed in this segment, IMPs in the proximal convoluted tubule were markedly smaller (5.1 ± 1.1 nm [n = 424]) than those in proteoliposomes and CHIP28k-transfected CHO cells. In the S3 segment of the proximal straight tubule, which was more heavily labeled with CHIP28 antibodies than the convoluted tubule (Nielsen et al., 1993; Sabolic et al., 1992), the IMPs were larger (Fig. 8 *b*); their average greatest diameter of 7.3 ± 1.6 nm (n = 390) was closer to that of the CHIP28 IMPs. The large IMPs in proximal straight tubules also included tetramers (Fig. 8 *b*, *inset*). Further analysis of the population of IMPs in proximal tubules is provided below.

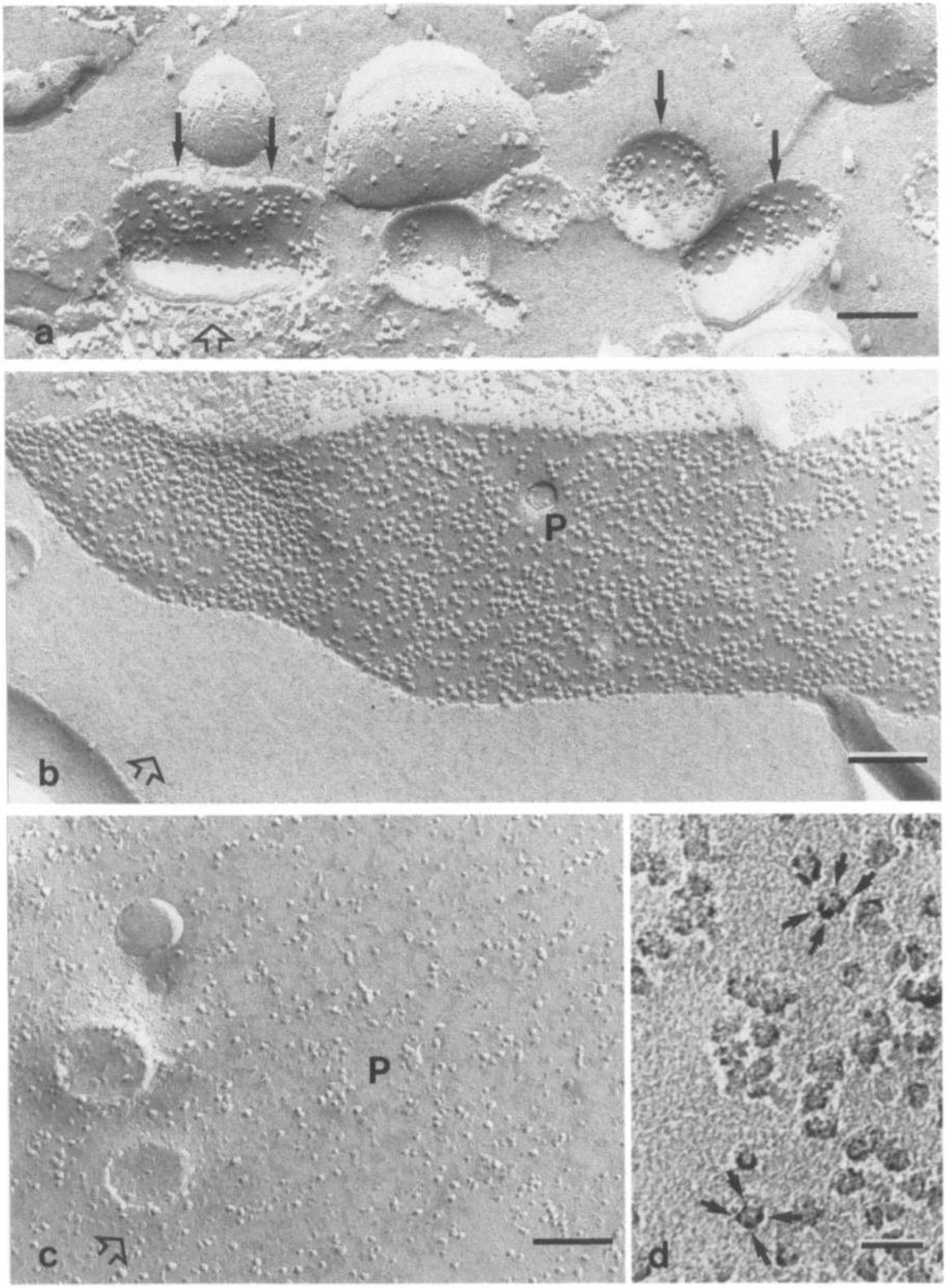

Figure 6. Freeze-fracture of intracellular membranes of CHIP28k-transfected CHO cells (*a*), CHIP28k-transfected cell plasma membrane P-face (*b*), and mock-transfected CHO cells plasma membrane P-face (*c*). Intracellular membranes (*full arrows*) and plasma membranes of CHIP28k-transfected cells contain additional large IMPs (*P*, P-face). Empty arrows show direction of platinum shadowing. (*d*) Rotary shadowing freeze-fracture of the CHIP28k-transfected CHO cell plasma membrane P-face demonstrates the presence of tetramers (*arrows*). Bars: (*a–c*) 100 nm; and (*d*) 20 nm.

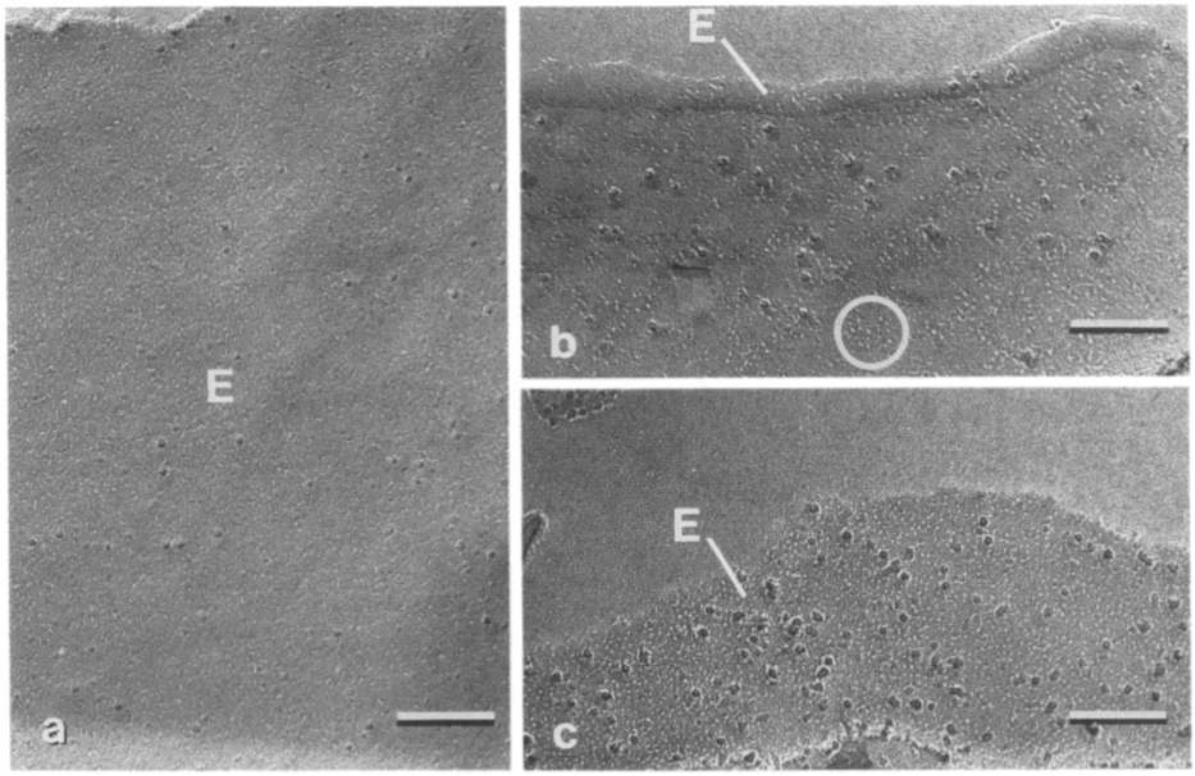

Figure 7. Rotary shadowing freeze–fracture of plasma membrane E-face (*E*) of thick ascending limb basolateral membrane (*a*), CHIP28k-transfected CHO cells (*b*), and thin descending long loop of Henle (*c*). A distinctive pattern of imprints, sometimes in loose clusters (*circle*) was observed on the plasma membrane E-face of cells containing CHIP28. Bars, 100 nm.

Table I. Comparison of P-face IMP Densities and E-face Imprints

Cell Type	Density of IMPs	Density of E-face imprints
	(*IMPs/μm²*)	(*imprints/μm²*)
Mock CHO cells	1282 ± 110 (18)	–
CHIP28k CHO cells	3682 ± 436 (14)	3834 ± 522 (8)
Thin descending limbs	7260 ± 1227 (6)	10036 ± 1363 (8)

IMP and imprint densities were measured on cell plasma membranes. Values are mean ± SD, with the number of cells in parenthesis: for each cell, IMPs (or imprints) were counted on a membrane surface area >0.02 μm^2 at ×190,000 magnification.

In the kidney, the most intense staining with anti-CHIP28 antibodies and the most intense hybridization with an antisense CHIP28k cRNA probe was obtained in thin descending limbs (TDL) (Nielsen et al., 1993; Sabolic et al., 1992; Zhang et al., 1993*a*). Therefore, we expected to find the highest density of CHIP28-associated IMPs in this nephron segment. As described previously (Orci et al., 1981), the P-face of both apical and basolateral plasma membranes in initial segments of TDL long loops had an extremely high density of IMPs, which were packed so closely together that very little particle-free membrane was visible (Fig. 8 *d*). As shown in Table I, the density of IMPs that we measured in rotary shadowed replicas was higher than previously published. This high degree of packing makes it difficult to resolve the structure of individual IMPs in freeze–fracture so that the actual density might be even higher. The population of IMPs observed in thin descending limbs (diameter 8.3 ± 1.3 nm [n = 260], Fig. 8 *d*) was more homogeneous than in other plasma membranes, including those containing a high density of IMPs of similar size such as basolateral membranes of thick ascending limbs (diameter 7.6 ± 2.1 nm [n = 368], Fig. 8 *c*). In TDL, many of the particles clearly appeared to be tetrameric (Fig. 8 *d*, *inset*).

As shown Fig. 7 *c*, the E-face of the TDL plasma membrane was decorated with the same pattern of ~2-nm imprints as seen in CHIP28k-transfected CHO cells (Fig. 7 *b*). This pattern was not observed on the plasma membrane E-face of cells that do not contain CHIP28, such as the basolateral membrane of thick ascending limb (Fig. 7 *a*), and probably reflects the extremely high density of CHIP28 protein in TDL. The density of these imprints on the E-face of TDL plasma membranes was measured (Table I) and found to be somewhat higher than the density of IMPs on the P-face. Because the E-face complementary imprints are more distinct than the P-face IMPs, their density is likely to represent a more accurate figure for the IMP density in the initial part of the TDL. In proximal tubule, where the density of CHIP28 is lower and where the IMP population is more heterogeneous, a similar network of imprints was not clearly visible on the plasma membrane E-face (Fig. 8, *a* and *b*).

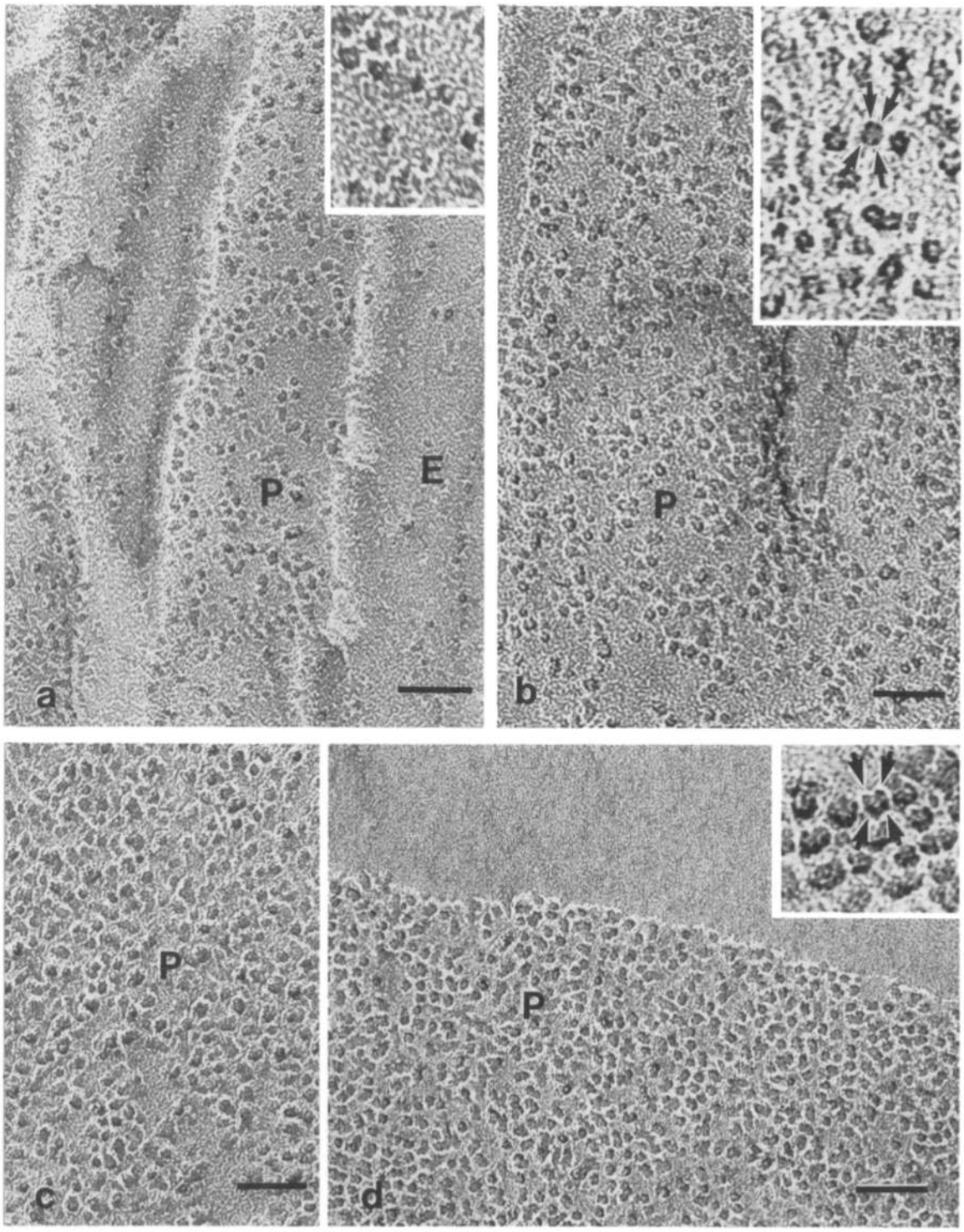

Figure 8. Rotary shadowing freeze-fracture of kidney cell plasma membranes. (*a*) Proximal convoluted tubule brush-border membrane. (*b*) S3 segment of the proximal straight tubule brush-border membrane. (*c*) Basolateral membrane of the thick ascending limb. (*d*) Thin descending limb of the loop of Henle (*long loop*) (*insets*, ×500,000). Tetramers of the size of CHIP28 were observed on the P-face (*P*) of S3 segment of the proximal tubule and in thin descending limb. Arrows show subunits of tetramer assemblies (*E*, E-face). Bars, 50 nm.

Quantitative Analysis of IMP Size Distribution

To quantify the morphological results presented in Figs. 3, 6, and 8, we measured the greatest diameter for >200 IMPs in the liposomes and cell plasma membranes. Histograms of IMP density versus diameter were constructed as shown in Fig. 9, and fitted to unimodal or bimodal Gaussian distributions. The parameters for the Gaussian regression are provided in Table III. The IMP size distribution in the liposomes reconstituted with CHIP28 (Fig. 9 *a*) was unimodal with a mean diameter of 8.5 nm. The size distribution in cell membranes containing CHIP28 was bimodal.

Table II. Comparison of CHIP28 IMP Densities and Water Permeability

	CHIP28 IMP density ($IMPs/\mu m^2$)	P_f (cm/s at 10°C)	
		predicted	measured
CHIP28k-transfected CHO cells	2,494	0.036	0.027
Proximal straight tubule	1,928	0.028	0.031
TDL	5,785	0.083	0.075*

The density of IMPs corresponding to CHIP28 was determined from the bimodal Gaussian analysis (see Materials and Methods and Fig. 9). Predicted P_f was calculated from the equation: $P_f = 4.D.p_f$, where D is the IMP density and p_f is the single CHIP28 channel monomer permeability of 3.6×10^{-14} cm^3/s at 10°C. Measured P_f was determined from the data in Fig. 1 *c*.

* To estimate plasma membrane P_f for TDL, the transepithelial P_f of ~2,000 $\mu m/s$ at 37°C (Chou and Knepper, 1992) was corrected for the apical plasma membrane folding factor (2.6 ± 0.7, mean ± SD) measured on 10 cells, for the presence of two permeability barriers in series of assumed equal P_f, and for the temperature dependence, using a 4 Kcal/mol activation energy.

The CHIP28k-transfected CHO cells had a remarkably higher density of IMPs than the mock-transfected cells (Table I); the diameter of the additional population of IMPs, representing CHIP28, was 8 to 9 nm (Fig. 9 *b*). The difference between IMP density in CHIP28 and mock-transfected CHO cells (Table I) was in good agreement with the CHIP28 IMP density fitted by non-linear regression (Table II). The thin descending limb plasma membrane showed a very high density of IMPs with a distribution similar to that found in CHIP28 liposomes, but very different from that observed in the water impermeable basolateral membrane of the thick ascending limb (Fig. 9 *c*). In the proximal tubule (Fig. 9 *d*), many IMPs of ~8-nm diam were observed in the S3 segment. In proximal convoluted tubule segments, where CHIP28 is less abundant, IMPs of ~8 nm did not represent a significant subpopulation. As discussed below in reference to Table II, there was good agreement of measured osmotic water permeability (P_f) in the CHIP28-containing membranes with P_f predicted from IMP density and single channel CHIP28 water permeability.

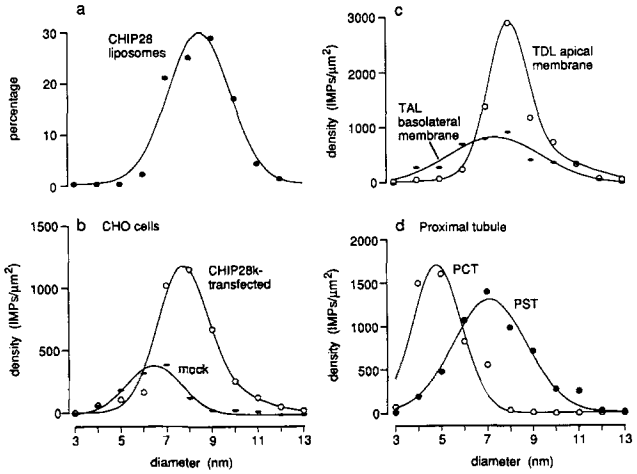

Figure 9. IMP size distribution. (*a*) CHIP28-incorporated proteoliposomes. (*b*) Plasma membranes in CHIP28k- and mock-transfected CHO cells. (*c*) Apical plasma membrane in native kidney thin descending limb and basolateral plasma membrane from kidney thick ascending limbs. (*d*) Apical plasma membrane from kidney proximal convoluted and proximal straight tubules. IMP densities were fitted to one or two Gaussian functions of the form: $y = \Sigma_i \alpha_i e^{-(x-\beta_i)^2/\sigma_i^2}$, where x is IMP diameter and y is density (see Table III below).

Discussion

The freeze-fracture technique has been useful for the study and characterization of several membrane proteins that possess unique morphological patterns, such as the IMP aggregates representing the vasopressin-sensitive water channel in amphibian urinary bladder (Chevalier et al., 1974; Kachadorian et al., 1975), the rod-shaped particles representing the H^+ ATPase in a number of cell types (Humbert et al., 1975; Orci et al., 1981; Wade, 1976), and gap junctions (Goodenough and Revel, 1970). In each case, an assembly of IMPs was observed on the P-face of freeze-fractured plasma membranes, and a distinct complementary imprint was located on the E-face. The formation of such structures is dependent on protein-protein and protein-lipid interactions. MIP26 is an interesting example of a protein that associates either in aggregated assemblies or in orthogonal arrays, both in native eye lens membranes and in proteoliposomes (Dunia et al., 1987; Zampighi et al., 1989).

We have studied by freeze-fracture EM the membrane as-

Table III.

Fitted Parameters	α_1	β_1	σ_1	α_2	β_2	σ_2	Total density
	($IMPs/\mu m^2$)	(*nm*)	(*nm*)	($IMPs/\mu m^2$)	(*nm*)	(*nm*)	($IMPs/\mu m^2$)
CHIP28 liposomes	30%*	8.5	1.8				–
Mock CHO cells	404	6.4	1.7				1,282
CHIP28 CHO cells	1,163	7.7	1.5	132	9.9	2.1	3,682
TAL	912	7.4	2.9				4,706
TDL	2,704	8.0	1.2	496	9.4	1.6	7,260
PCT	1,626	4.8	1.5				4,344
PST	343	7.8	1.5	921	7.1	2.5	5,048

TAL, Thick ascending limb basolateral membrane; *TDL*, thin descending limb; *PCT*, proximal convoluted tubule; and *PST*, proximal straight tubule.
* In liposomes, unit is percentage of total IMPs measured.

sociation of the CHIP28 water channel. CHIP28 did not form clusters either in cell membranes or in liposomes, unlike MIP26, which belongs to the same family of transmembrane channels. The average IMP size measured in CHIP28-reconstituted proteoliposomes was 8.5 ± 1.3 nm. A subpopulation of IMPs of the same size was found on the plasma membrane P-face of each of the CHIP28-containing cell types that we examined. IMP imprints were found on the E-face of the cell membranes that contain a high density of CHIP28 water channels, and on proteoliposomes reconstituted with purified CHIP28.

As previously suggested by sedimentation analysis and SDS-PAGE analysis of glutaraldehyde cross-linked CHIP28 (Smith and Agre, 1991), we found by the freeze-fracture technique that human erythrocyte CHIP28 was associated as oligomers both in *N*-lauroylsarcosine–stripped membranes containing primarily CHIP28 and in proteoliposomes reconstituted with purified CHIP28. The IMPs observed on either face of the vesicle membranes were consistently made up of four subunits, resulting in a relatively large assembly of ~8.5-nm diam with an apparent central depression. As shown in Fig. 10, a simple geometric model for such a tetramer consists of four CHIP28 monomers arranged symmetrically. Assuming that each monomer is a right cylinder of 5-nm length and that the protein density is 1.3 g/cm^3, then each CHIP28 monomer would have a diameter of 3 nm. The greater diameter of the smallest square tetrameric assembly would be 7.2 nm. When the total thickness of platinum in the replicas (~1.5 nm) is added, the predicted IMP diameter of ~8.7 nm is in good agreement with the observed diameter of ~8.5 nm. Interestingly, MIP26 was also reported to form tetrameric IMPs of ~8 nm in liposomes (Dunia et al., 1987). In native membranes and liposomes, MIP26 is associated in orthogonal arrays of IMPs with a spacing of ~7 nm (Dunia et al., 1987; Zampighi et al., 1989). This value, which probably represents the size of MIP26 tetramers without the platinum coat, is similar to the predicted size of CHIP28 tetramers. Our model for CHIP28 would predict a central depression of ~1.2 nm; similar central depressions have been reported for other types of IMPs in several cells, and were interpreted to represent hydrophilic channels (Orci et al., 1977). In the case of CHIP28, however, there is evidence that the functional water channel unit is the monomer. Target size determination by radiation inactivation gave a functional unit size of ~30 kD for both erythrocyte and kidney proximal tubule water channels (Van Hoek et al., 1991). In addition, permeability measurements in oocytes coexpressing wild-type and mutant CHIP28 cRNAs suggested a monomeric functional subunit (Preston et al., 1993; Zhang et al., 1993*b*). Taken together, these data suggest that functionally independent CHIP28 monomers are assembled in membranes as tetramers of ~7.2-nm diam. The tetrameric assembly is probably driven by monomer–monomer electrostatic interactions to give an oligomer size having minimum free energy.

A CHO cell line transfected with CHIP28k cDNA was used to examine the structure and distribution of CHIP28 in mammalian cell membranes. The increase in water permeability in the CHIP28k-transfected cells and the immunolocalization of CHIP28k correlated, by freeze–fracture EM, with an increased density of IMPs on the plasma membrane P-face. The large additional population of IMPs in CHIP28k-transfected cells, also observed in some intracellular membranes, was homogeneous and had a larger average diameter than the IMPs found in mock-transfected cells. This subpopulation of IMPs representing the CHIP28 water channel had approximately the same size and shape as those in reconstituted proteoliposomes.

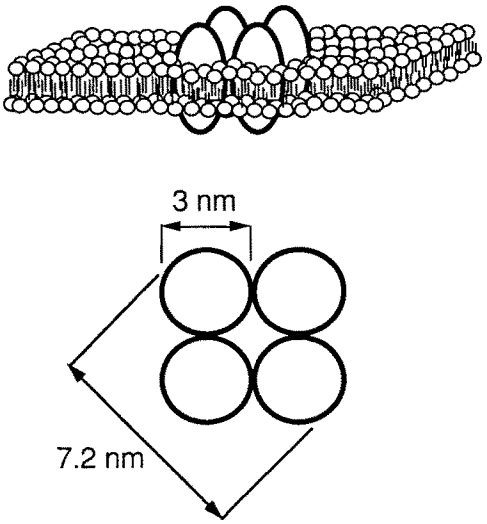

Figure 10. Model for CHIP28 assembly in membranes. IMPs representing CHIP28 in freeze-fracture EM are consistent with a symmetrical assembly of four CHIP28 monomers with a central depression. See text for explanation.

An interesting complement to the P-face IMPs associated with CHIP28 was observed on the E-face of the CHIP28k-transfected CHO cells. The complementary pattern of CHIP28 IMPs on the E-face, observed only in transfected cells, was visualized as highly contrasted imprints. These imprints had the same density and distribution on the membrane E-face as the IMPs on the complementary P-face, and are probably each produced by a single CHIP28 IMP. Indeed, similar imprints were found on the membrane of liposomes that contain CHIP28. The reason why CHIP28 leaves such a recognizable imprint on the plasma membrane E-face is not known, although it has been previously reported that other types of IMPs leave characteristic imprints on the corresponding E-face. These include rod-shaped IMPs that are associated with the proton pumping ATPase (Humbert et al., 1975; Wade, 1976), connexons that form gap junction subunits (Goodenough and Revel, 1970), square arrays of IMPs of unknown function, but that are morphologically similar to MIP26, in a variety of cell types (Orci et al., 1981), and IMP aggregates that are believed to represent vasopressin-sensitive water channels in amphibian bladder (Kachadorian et al., 1975). MIP26 also leaves imprints in lens membranes and in proteoliposomes (Dunia et al., 1987; Zampighi et al., 1989). It has been suggested that IMPs that do leave such a depression on the E-face may be composed of protein complexes that are very rich in lipid (Ververgaert and Verkleij, 1978). Like MIP26, CHIP28 is a very hydrophobic protein that is predicted to be tightly associated with membrane lipids in situ (Van Hoek et al., 1993).

Finally, we examined the membrane assembly of CHIP28 in rat kidney proximal tubule and thin descending limb of Henle. As described previously, the plasma membranes of

these nephron segments contain a high density of IMPs. In proximal tubule, CHIP28 was previously localized to S2 and S3 segments (Nielsen et al., 1993; Sabolic et al., 1992). Despite the heterogeneity of membrane proteins and associated IMPs in proximal tubule, we found differences in the density and size distribution of IMPs between proximal convoluted tubules and the S3 segment of proximal straight tubules. In particular, IMPs of size compatible with CHIP28 (8 to 9 nm) were numerous in proximal straight tubules, but did not represent a distinct subpopulation in the convoluted tubules that we examined. This observation is consistent with the weak labeling of the S1 segment of proximal tubules by immunocytochemistry.

Unlike the findings in CHIP28k-transfected CHO cells, we did not detect any remarkable pattern of imprints on the E-face of proximal tubule plasma membranes. In this segment, the IMPs are heterogeneous and the amount of membrane-associated CHIP28 is probably considerably less than in transfected cells.

Of all CHIP28-containing cells, the highest level of antibody labeling and antisense cRNA probe hybridization was found in thin descending limbs of Henle (Hasegawa et al., 1993; Nielsen et al., 1993; Sabolic et al., 1992). Functional studies have demonstrated that the upper part of TDL long loops is highly water permeable (Chou and Knepper, 1992). By freeze-fracture EM, this segment of the TDL was found to contain the highest density of IMPs of all kidney epithelial cells on both apical and basolateral plasma membranes (Orci et al., 1981). In contrast, water impermeable segments of the TDL contain low densities of IMPs in their plasma membranes. We found that the IMP size distribution and subunit assembly in the upper part of TDL long loops was similar to that of the purified CHIP28 in reconstituted proteoliposomes. In addition, the characteristic E-face network of imprints found in CHIP28k-transfected cells was also observed in the TDL. Unlike in CHO cells where both the IMPs and imprints were sometimes found in loose clusters, the imprints were evenly distributed on the TDL plasma membrane E-face. The average spacing of these imprints (~10 nm), complementary to P-face IMPs of ~8.3-nm diam, reflects the high density of IMPs on TDL plasma membranes.

The quantitative analysis of IMP density versus greatest diameter provided strong support for the conclusion that the characteristic size of IMPs representing CHIP28 was ~8.5 nm. IMPs of this size were observed in reconstituted proteoliposomes, CHIP28-transfected CHO cells, and those native kidney cell plasma membranes that are known to have high water permeability. It is important to note that quantitative studies of IMP size in freeze-fracture EM are limited for several reasons. In addition to measurement errors, there are variations in the thickness of platinum coat, in the accuracy of electron microscope magnification (Elbers and Pieters, 1964), and in the orientation of membranes and IMPs during shadowing and observation. As demonstrated on stereomicrographs, because of the curvature of the membrane, the orientation of IMPs in liposomes is particularly heterogeneous. This probably accounts for the wider IMP size distribution found in reconstituted proteoliposomes than in TDL. Despite these caveats, the analysis of IMP size distribution by non-linear regression on a large number of samples provided a useful quantitative approach to analyze and compare IMP geometry in a variety of cell types, and to estimate CHIP28 density.

It is interesting to compare P_f measured in CHO cells and native kidney membranes with that predicted by the analysis of IMP size and number. The predicted P_f (in cm/s) is given by the product of single channel p_f (3.6×10^{-14} cm^3/s per CHIP28 monomer at 10°C), and CHIP28 density (monomers/μm^2). Table II shows the comparison. In CHO cells and in TDL, a large proportion of IMPs represent CHIP28. Therefore, the comparison of measured and predicted P_f's is independent of the bimodal Gaussian model used to fit the IMP distribution in these cell types. In the stably transfected CHO cells, P_f measured in isolated plasma membrane vesicles (devoid of unstirred layer effects because of their small size) was 0.027 cm/s, in good agreement with P_f of 0.036 cm/s predicted from the CHIP28 IMP density. In native kidney membranes, predicted and measured P_f values also agreed quite well. The predicted P_f (0.028 cm/s) calculated from the density of IMPs representing CHIP28 in the proximal straight tubule was similar to the value of 0.031 measured in rat renal brush-border vesicles. As described in Table II, the plasma membrane P_f for the thin descending limb was estimated from the transepithelial P_f of ~0.2 cm/s at 37°C (Chou and Knepper, 1992) to be 0.075 cm/s at 10°C. This value agreed well with the predicted P_f of 0.083 cm/s. The density of 5785 CHIP28 tetramers/μm^2 found in the water permeable initial segment of the rat TDL is remarkably high. Using the calculated weight of each CHIP28 tetramer (1.9×10^{-19} g), and the plasma membrane density of $\sim 5 \times 10^{-15}$ g/μm^2, CHIP28 probably accounts for ~22% of the total membrane weight. This result suggests that the initial part of rat TDL is highly specialized in water transport.

In conclusion, our results provide evidence that CHIP28 is represented in freeze-fracture EM by tetrameric IMPs of ~8.5 nm greatest diameter in artificial membranes, transfected cells, and native cell plasma membranes. This freeze-fracture appearance of CHIP28 is distinct from that of closely related protein MIP26, which forms tetrameric orthogonal arrays of IMPs in membranes.

This work was supported by National Institute of Diabetes and Digestive and Kidney Diseases Grants DK-38452, and DK-35124 and a grant-in-aid from the American Heart Association. A. S. Verkman is an Established Investigator of the American Heart Association.

Received for publication 30 April 1993 and in revised form 21 July 1993.

References

Biber, J., B. Steiger, W. Haase, and H. Murer. 1981. A high yield preparation for rat kidney brush border membranes. *Biochim. Biophys. Acta.* 647: 169–176.

Brown, D., A. Grosso, and R. C. DeSousa. 1983. Correlation between water flow and intramembrane particle aggregates in toad epidermis. *Am. J. Physiol.* 245:C334–C342.

Chevalier, J., J. Bourguet, and J. S. Hugon. 1974. Membrane associated particles: Distribution in frog urinary bladder epithelium at rest and after oxytocin treatment. *Cell Tissue Res.* 152:129–140.

Chou, C.-L., and M. A. Knepper. 1992. *In vitro* perfusion of chinchilla thin limb segments: segmentation and osmotic water permeability. *Am. J. Physiol.* 263:F417–F426.

Deen, P. M., J. A. Dempster, B. Wieringa, and C. H. van Os. 1992. Isolation of a cDNA for rat CHIP28 water channel: high mRNA expression of kidney cortex and inner medulla. *Biochem. Biophys. Res. Commun.* 188:1267–1273.

Denker, B. M., B. L. Smith, F. P. Kuhajda, and P. Agre. 1988. Identification, purification, and partial characterization of a novel Mr 28,000 integral membrane protein from erythrocytes and renal tubules. *J. Biol. Chem.* 263: 15634–15642.

Dunia, I., S. Manenti, A. Rousselet, and E. L. Benedetti. 1987. Electron microscopic observations of reconstituted proteoliposomes with the purified major

intrinsic membrane protein of eye lens fibers. *J. Cell Biol.* 105:1679–1689.
Elbers, P. F., and J. Pieters. 1964. Accurate determination of magnification in the electron microscope. *J. Ultrastruct. Res.* 11:25–32.
Goodenough, D. A., and J.-P. Revel. 1970. A fine structural analysis of intercellular junctions in the mouse. *J. Cell Biol.* 45:272–290.
Green, R., and G. Giebisch. 1989. Reflection coefficients and water permeability in rat proximal tubule. *Am. J. Physiol.* 257:F658–F668.
Harmanci, M. C., P. Stern, W. A. Kachadorian, H. Valtin, and V. A. DiScala. 1978. Antidiuretic hormone-induced intramembranous alteration in mammalian collecting ducts. *Am. J. Physiol.* 235:F440–F443.
Hasegawa, H., R. Zhang, A. Dohrman, and A. S. Verkman. 1993. Tissue-specific expression of mRNA encoding rat kidney water channel CHIP28k by in situ hybridization. *Am. J. Physiol.* 264:C237–C245.
Humbert, F., C. Pricam, A. Perrelet, and L. Orci. 1975. Specific plasma membrane differentiations in the cells of the kidney collecting tubule. *J. Ultrastruct. Res.* 52:13–20.
Kachadorian, W. A., J. B. Wade, and V. A. DiScala. 1975. Vasopressin: induced structural change in toad bladder luminal membrane. *Science (Wash. DC).* 190:67–69.
Ma, T., A. Frigeri, S.-T. Tsai, J.-M. Verbavatz, and A. S. Verkman. 1993. Localization and functional analysis of CHIP28k water channels in stably transfected CHO cells. *J. Biol. Chem.* In press.
Nielsen, S., B. L. Smith, E. I. Christensen, M. A. Knepper, and P. Agre. 1993. CHIP28 water channels are localized in constitutively water-permeable segments of the nephron. *J. Cell Biol.* 120:371–383.
Orci, L., A. Perrelet, F. Malaisse-Lagae, and P. Vassalli. 1977. Pore-like structures in biological membranes. *J. Cell Sci.* 25:157–162.
Orci, L., F. Humbert, D. Brown, and A. Perrelet. 1981. Membrane ultrastructure in urinary tubules. *Int. Review Cytol.* 73:183–241.
Preston, G. M., and P. Agre. 1991. Isolation of the cDNA for erythrocyte integral membrane protein of 28 kilodaltons: member of an ancient channel family. *Proc. Natl. Acad. Sci. USA.* 88:11110–11114.
Preston, G. M., T. P. Carroll, W. B. Guggino, and P. Agre. 1992. Appearance of water channels in *Xenopus* oocytes expressing red cell CHIP28 protein. *Science (Wash. DC).* 256:385–387.
Preston, G. M., J. S. Jung, W. B. Guggino, and P. Agre. 1993. The mercury-sensitive residue at cysteine 189 in the CHIP28 water channel. *J. Biol. Chem.* 268:17–20.
Sabolic, I., G. Valenti, J.-M. Verbavatz, A. N. van Hoek, A. S. Verkman, D. A. Ausiello, and D. Brown. 1992. Localization of the CHIP28 water channel in rat kidney. *Am. J. Physiol.* 263:C1225–C1233.
Schafer, J. A., C. S. Patlak, S. L. Troutman, and T. E. Andreoli. 1978. Volume absorption in the pars recta. II. Hydraulic conductivity coefficient. *Am. J. Physiol.* 234:F340–F348.
Smith, B. L., and P. Agre. 1991. Erythrocyte Mr 28,000 transmembrane protein exists as multisubunit oligomer similar to channel proteins. *J. Biol. Chem.* 266:6407–6415.
Van Hoek, A. N., and A. S. Verkman. 1992. Functional reconstitution of the isolated erythrocyte water channel CHIP28. *J. Biol. Chem.* 267:18267–18269.
Van Hoek, A. N., M. L. Hom, L. H. Luthjems, M. D. de Jong, J. A. Dempster, and C. H. van Os. 1991. Functional unit of 30kDa for proximal tubule water channels as revealed by radiation inactivation. *J. Biol. Chem.* 226:16633–16635.
Van Hoek, A. N., M. Wiener, S. Bicknese, L. Miercke, J. Biwersi, and A. S. Verkman. 1993. Secondary structure analysis of purified functional CHIP28 water channels by CD and FTIR spectroscopy. *Biochemistry.* In press.
Verkleij, A. J., and P. H. J. T. Ververgaert. 1978. Freeze-fracture morphology of biological membranes. *Biochim. Biophys. Acta.* 515:303–327.
Ververgaert, P. H. J. T., and A. J. Verkleij. 1978. A view on intramembraneous particles. *Experientia.* 34:454–456.
Wade, J. B. 1976. Membrane structural specialization of the toad urinary bladder revealed by the freeze-fracture technique. II. The mitochondria-rich cell. *J. Membr. Biol.* 29:111–126.
Zampighi, G. A., J. E. Hall, G. R. Ehring, and S. A. Simon. 1989. The structural organization and protein composition of lens fiber junctions. *J. Cell Biol.* 108:2255–2275.
Zeidel, M. L., S. V. Ambudkar, B. L. Smith, and P. Agre. 1992. Reconstitution of functional water channels in liposomes containing purified red cell CHIP28 protein. *Biochemistry.* 31:7436–7440.
Zhang, R., W. Skach, H. Hasegawa, A. N. van Hoek, and A. S. Verkman. 1993*a*. Cloning, functional analysis and cell localization of a kidney proximal tubule water transporter homologous to CHIP28. *J. Cell Biol.* 120: 359–370.
Zhang, R., A. N. van Hoek, J. Biwersi, and A. S. Verkman. 1993*b*. A point mutation at cysteine 189 blocks the water permeability of rat kidney water channel CHIP28k. *Biochemistry.* 32:2938–2941.